Effect of composition on the spontaneous emission probabilities, stimulated emission cross-sections and local environment of Tm^{3+} in TeO_2–WO_3 glass

G. Özen[a,*], A. Aydinli[b], S. Cenk[c], A. Sennaroğlu[d]

[a] Faculty of Science and Letters, Department of Physics, Istanbul Technical University, Maslak, 80626, Istanbul, Turkey
[b] Physics Department, Bilkent University, 06533 Bilkent-Ankara, Turkey
[c] TUBİTAK-Marmara Research Center, 41470 Gebze-Kocaeli, Turkey
[d] Physics Department, Koc University, 80860 Istinye-Istanbul, Turkey

Abstract

Effect of composition on the structure, spontaneous and stimulated emission probabilities of various $1.0\,mol\%$ Tm_2O_3 doped $(1-x)TeO_2+(x)WO_3$ glasses were investigated using Raman spectroscopy, ultraviolet–visible–near-infrared (UV/VIS/NIR) absorption and luminescence measurements.

Absorption measurements in the UV/VIS/NIR region were used to determine spontaneous emission probabilities for the 4f–4f transitions of Tm^{3+} ions. Six absorption bands corresponding to the absorption of the $^1G_4$, $^3F_2$, $^3F_3$ and $^3F_4$, $^3H_5$ and $^3H_4$ levels from the $^3H_6$ ground level were observed. Integrated absorption cross-section of each band except that of $^3H_5$ level was found to vary with the glass composition. Luminescence spectra of the samples were measured upon 457.9 nm excitation. Three emission bands centered at 476 nm ($^1G_4 \rightarrow {}^3H_6$ transition), 651 nm ($^1G_4 \rightarrow {}^3H_4$ transition) and 800 nm ($^1G_4 \rightarrow {}^3H_5$ transition) were observed. Spontaneous emission cross-sections together with the luminescence spectra measured upon 457.9 nm excitation were used to determine the stimulated emission cross-sections of these emissions.

The effect of glass composition on the Judd–Ofelt parameters and therefore on the spontaneous and the stimulated emission cross-sections for the metastable levels of Tm^{3+} ions were discussed in detail. The effect of temperature on the stimulated emission cross-sections for the emissions observed upon 457.9 nm excitation was also discussed.
© 2002 Elsevier Science B.V. All rights reserved.

Keywords: Tellurite glass; Thulium; Intensity parameters; Composition

1. Introduction

Technological development of the optical tele-communications based on the growth of technol-ogies of fiber fabrication and the laser diode (LD) has enabled efficient pumping of rare-earth ions such as Pr^{3+}, Nd^{3+} and Er^{3+} [1]. In these systems,

*Corresponding author. Tel.: +90-21-2285-3206; fax: +90-21-2285-6386.

E-mail address: gozenl@itu.edu.tr (G. Özen).

there are a number of interesting relationships between the active ions and the host glass [2]. Among these, glasses with low phonon energies are of interest as hosts for infrared and infrared to visible upconversion lasers [3]. Since the oxide glasses such as silicate, borate and phosphate glasses have high phonon energies, in these glasses the multiphonon relaxation becomes the dominant relaxation process for transitions with small energy gaps. On the other hand, there are some oxide glasses with low phonon energies such as tellurite and gallate in which upconversion fluorescence of Er^{3+} was observed [4]. Although fluoride glasses have even lower phonon energies which allow weak self-quenching as shown for the Nd^{3+} case by Michel et al. [5], they lack many of the desirable features of tellurite glasses including mechanical strength and chemical durability [6]. Tellurite glasses, compared with silicate and borate and fluoride glasses, have more advantages as laser hosts due to their superior physical properties such as low melting temperature [6–8], high dielectric constant [9,11], high refractive index [9,10], large third order nonlinear susceptibility [12,13] and good infrared transmissivity [14]. Furthermore, they present large transparency from the near ultraviolet to the middle infrared region. They are resistant to atmospheric moisture and capable of incorporating large concentrations of rare-earth ions into the matrix [15].

One of the important properties for the evaluation of the host glasses is the spontaneous emission probability for the 4f–4f transitions of the rare-earth ions in them. Spontaneous emission probability of the laser transition is an important parameter because it is directly related to the stimulated emission cross-section, radiative quantum efficiency, and fluorescence branching ratio [16]. The Judd–Ofelt theory is usually used to determine the electric dipole transition probabilities including the spontaneous decay rate by utilising the absorption cross-sections of several 4f–4f transitions [17,18]. The spontaneous emission probability is affected mainly by the sum of products of intensity parameters, Ω_t ($t = 2, 4, 6$) and doubly reduced matrix elements of tensor operators, $U^{(t)}$. For example, Takebe et al. [19] reported that the spontaneous emission probabil-

ities of the transitions $^1G_4 \rightarrow {}^3H_5$ of Pr^{3+} at 1.3 µm, $^4F_{3/2} \rightarrow {}^4I_{11/2}$ of Nd^{3+} at 1.06 µm and $^4I_{13/2} \rightarrow {}^4I_{15/2}$ of Er^{3+} at 1.5 µm depend mainly on the $\Omega_6 \left(|\langle \| U^{(6)} \| \rangle \right)^2$ term, where only the Ω_6 is related to the glass composition. Optimisation of the glass composition with respect to the intensity parameters, Ω_t, is desirable to obtain higher values of the spontaneous emission probabilities for the appropriate active ions.

Until now, the optical amplifiers have been made of rare-earth doped fluoride, phosphate [5] and silica glasses although the latter glasses' phonon cut-off frequency is high [20,21]. Several researchers have also pointed out that SiO_2 is not a suitable host for rare-earth ions because the ions tend to form clusters in the silica network. This clustering results in the concentration quenching of luminescence due to the cross-relaxation processes between the neighboring ions [22]. It is reported that the gain band of 40 nm at 1.5 µm has been achieved in Er^{3+} doped alumino-silicate glass host in which aluminum oxide reduces the clustering of rare-earth ions [22]. Recently it is also reported that the bandwidth of 80 nm has been achieved in a tellurite glass host [23].

It is known that, unlike SiO_2 glasses, addition of elements like WO_3 is needed to form TeO_2-based bulk glasses [24]. Glass forming regions together with some physical and thermal properties of various TeO_2-based glasses have been reported [25–29,33]. There exists also several investigations on the optical and photoluminescence properties of Eu^{3+}, Yb^{3+}, Nd^{3+}, and Er^{3+} doped tellurite glasses [30–32]. No studies, however, have been found concerning the glasses of TeO_2–WO_3–Tm_2O_3 system.

In this study, the effect of WO_3 content on the structure and the 4f–4f spontaneous and stimulated transition probabilities of 1.0 mol% Tm^{3+} in $(1-x)TeO_2 + (x)WO_3$ glasses were investigated by means of Raman spectroscopy, ultraviolet–visible–near-infrared (UV/VIS/NIR) absorption and luminescence measurements at room temperature. The effect of temperature on the blue emission due to $^1G_4 \rightarrow {}^3H_6$ transition, which could be used as the upconversion laser emission when $^3F_4$ level is pumped via $^3F_3$ level using 650 nm light, was also investigated.

2. Experimental

2.1. Glass synthesis

Tellurite glasses were prepared with the compositions of $(1-x)TeO_2+(x)WO_3$ where $x = 0.15$, 0.25, 0.30 in molar ratio. A series of 1.0 mol% Tm_2O_3 doped glasses were also prepared using the same temperature arrangement used for the preparation of the undoped glasses. All chemicals used were reagent grade of TeO_2 (99.999% purity, Aldrich Chemical Company), WO_3 (99.99% purity, Merck Chemical Company), and Tm_2O_3 (99.9% purity Sigma Chemical Company). Batches of 7 g size were thoroughly mixed and melted in a platinum crucible at $800-950°C$ for 30 min in an electrically heated furnace in air atmosphere. The glass melts were removed from the furnace at $950°C$ and then air quenched by pressing between two rectangular graphite slabs at room temperature.

2.2. Optical measurements

Optical absorption of the glasses having the thickness of 2 ± 0.1 mm were recorded with a Shimadzu UV–VIS–NIR 3101 PC spectrometer in the wavelength range of 300–2000 nm. The measurements were carried out at room temperature.

Raman and photoluminescence experiments were carried out on samples in a back scattering configuration in the wavelength range of 460–860 nm. The 457.9 nm (2.71 eV) line of an argon ion laser was used as the exciting light source. The luminescence was analyzed with a U-1000 Jobin-Yvon double grating monochromator and cooled GaAs photomultiplier tube with the standard photon counting electronics. A CTI-Cryogenics M-22 closed-cycle helium cryostat was used to cool the samples from room temperature down to 9 K. Temperature was controlled to within an accuracy of ±0.5 K. A cylindrical lens was used in focusing optics in order to minimise unnecessary heating of the sample by the incident laser beam. All spectra have been corrected for the spectral response of the optical apparatus.

3. Results and discussion

3.1. Judd–Ofelt intensity parameters and spontaneous emission probabilities

Absorption spectrum of 1 mol% Tm_2O_3 doped $(0.70)TeO_2+(0.15)WO_3$ glass is presented in Fig. 1. The spectrum shows six bands peaked at
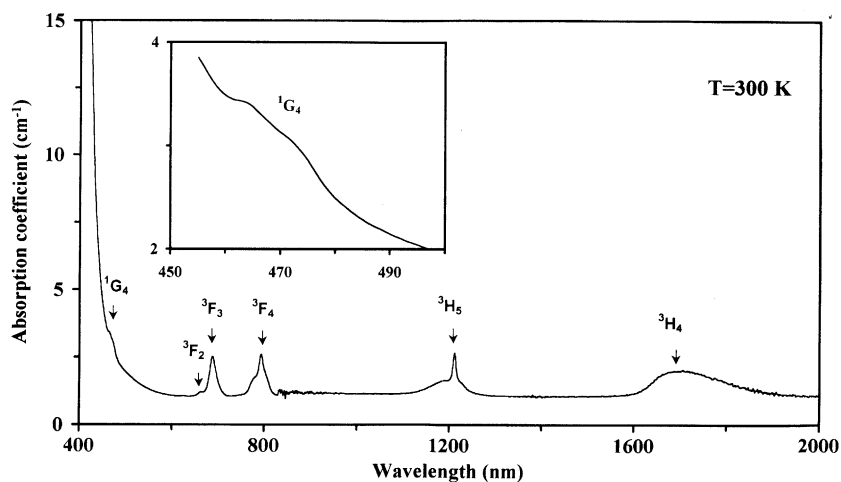

Fig. 1. Absorption spectrum of $(0.85)TeO_2+(0.15)WO_3$ glass doped with 1 mol% Tm_2O_3 at room temperature.

458, 660, 686, 794, 1212 and 1670 nm corresponding to the ground state absorptions of $^1G_4$, $^3F_2$, $^3F_3$, $^3F_4$, $^3H_5$, and $^3H_4$ levels, respectively. The positions of the absorption peaks for these glasses are very similar to thulium doped fluorozirconate-based glass, e.g., ZBLA [34,35], and are therefore shifted only slightly from thulium silicates [36]. From the spectra it can be seen that the absorption into the $^1G_4$ level has a double peak structure, unseen either in fluorozirconate based or silica based thulium hosts, indicating rather well defined local environments around Tm^{3+} in $TeO_2 + WO_3$ glass.

Fig. 2 shows the effect of the glass composition on the spectral profiles of the absorption bands. The profile and the peak position of each transition remain unchanged. However, the integrated absorption cross-section of all the bands except that of corresponding to the $^3H_6 \rightarrow ^3H_5$

transition shows a dependence on the glass composition.

Absorption cross-section of a ground state absorption, σ_{abs}, is given by

$$\sigma_{abs} \; (cm^{-2}) = \frac{2.303 \log(I_o/I)}{cl}, \tag{1}$$

where $\log(I_o/I)$ is the absorbance, l is the thickness of the sample in cm, and c is the Tm^{3+} concentration per cm^3 in the glass . The Tm^{3+} concentrations were calculated from the densities and the batch compositions of the samples. Density of each glass was determined by the Archimed's method using distilled water as an immersion liquid. The absorption cross-section for the ground state absorption bands of each level was integrated using the following equation:

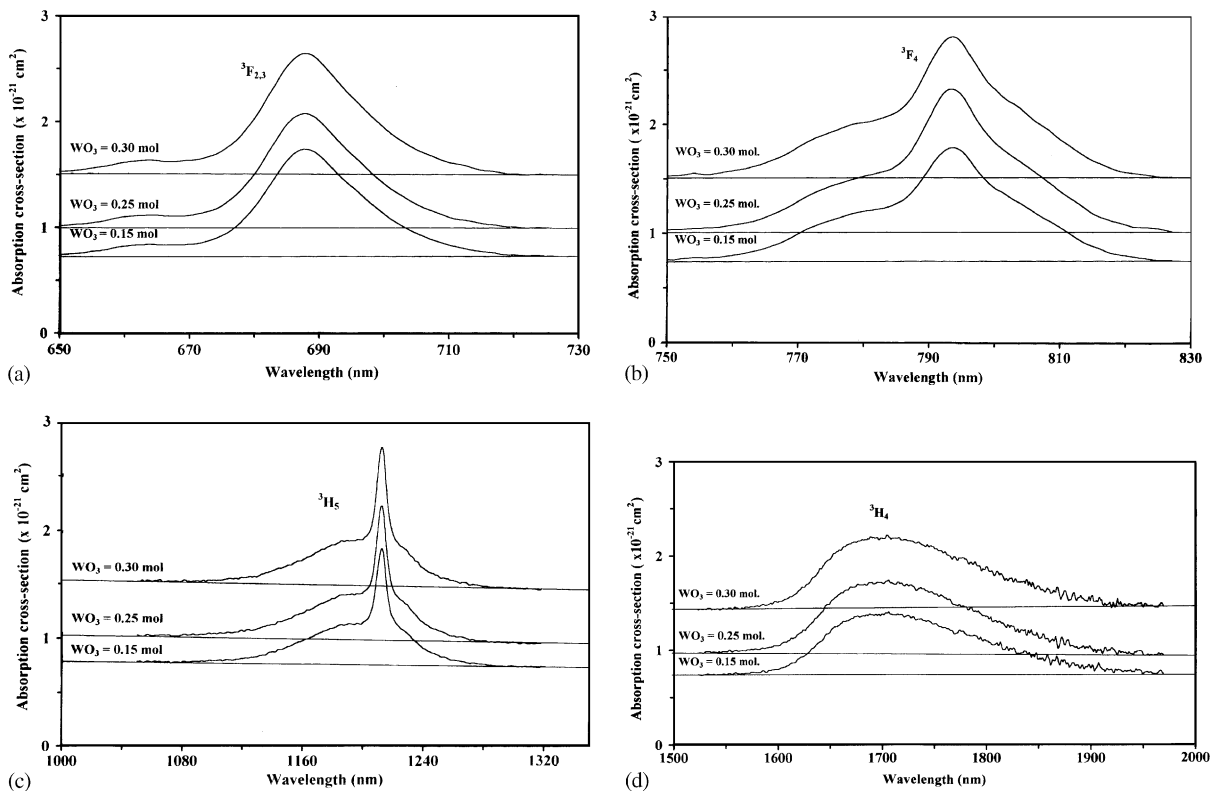$$\sum_{abs} = \int \sigma_{abs}(\lambda) \, d\lambda, \tag{2}$$

Fig. 2. Effect of the glass composition on the spectral profiles of the absorption bands for (a) $^3H_6 \rightarrow ^3F_{2,3}$, (b) $^3H_6 \rightarrow ^3F_4$, (c) $^3H_6 \rightarrow ^3H_5$, and (d) $^3H_6 \rightarrow ^3H_4$ transitions.

where $\sum_{abs}$ is the integrated absorption cross-section. Results are given in Table 1. Integrated absorption cross-section of all the levels except $^3H_5$ level varies considerably with the WO_3 content. Strongest variation is observed in that of $^3H_4$ level with 246×10^{-28} and $328 \times 10^{-28}\,cm^3$ for 0.15 and $0.30\,mol\,WO_3$ content, respectively.

Spectral intensity, also called integrated absorbance, for the observed absorption bands were determined experimentally using the following formula:

$$f_{exp} = \int_{band} \mu(\lambda)\,d\lambda, \qquad (3)$$

where $\mu(\lambda)$ is the absorption coefficient and is given by; $\mu(cm^{-1}) = [\sigma_{abs}{}^*c]$.

The Judd–Ofelt [17,18] theory relates the theoretically determined oscillator strength, f_{cal}, of a transition from the ground state to an excited state with the integrated absorbance of the transition. If the transition is electric-dipole type then, the calculated oscillator strength for an electric dipole transition from the ground state ($\langle SLJ|$) to an excited state ($|S'L'J'\rangle$) is given by

$$f_{cal}(J,J') = \frac{8\pi^2 m\bar\lambda}{3h(2J+1)}\left[\frac{(n^2+2)^2}{9n}S'_{ed} + nS'_{md}\right], \quad (4)$$

where $\bar\lambda$ is the mean wavelength for the absorption bands (or bands in the case of overlapping Stark manifolds), n is the refractive index of the relevant glass, J is the degeneracy of the ground state and S'. The value of the refractive index was taken as 2.17 and 2.16 for the glasses having 15 and 20 mol% and, 2.16 mol%, respectively [24]. Since the reduced matrix elements, $U^{(t)}$, are not strongly host dependant we have used the values calculated by Kaminskii in LaF_3 [37]. The three Judd–Ofelt intensity parameters, Ω_t, were obtained by least squares fitting of our experimentally determined oscillator strength to the $U^{(t)}$ matrix elements, and are given in Table 2. Theoretical f_{cal}-values were then determined by using Eq. (4) and, are presented in Table 3 together with the measured oscillator strengths. The r.m.s. deviation of the f-calculated from the f-measured values determined from the residuals is also presented in Table 3.

Spontaneous emission probability for a $SLJ \rightarrow S'L'J'$ electric dipole emission is calculated from the following equation:

$$A(J,J') = \frac{64\pi^4 e^2}{3(2J+1)h}\frac{n(n^2+2)^2\bar\nu^3}{9}$$
$$\times \sum_{t=2,4,6} \Omega_t \left(\langle SLJ||U^{(t)}||S'L'J'\rangle\right)^2, \quad (5)$$

Table 1
Compositional dependence of integrated absorption cross-section of Tm^{3+} ground state absorption bands

Glass composition (mol%)			$\int \sigma(\lambda)\,d\lambda = \int_{band}\frac{2.303\log(I(\lambda)/I_o)}{cl}\,d\lambda$ ($\times 10^{-28}\,cm^3$)			
TeO_2	WO_3	Tm_2O_3	$^3F_{2+3}$	$^3F_4$	$^3H_5$	$^3H_4$
85	15	1	50.0	61.0	93.0	246.0
75	25	1	56.0	73.0	108.0	309.0
70	30	1	52.0	72.0	110.0	328.0

Table 2
Compositional dependence of the Judd–Ofelt intensity parameters

Glass composition (mol%)			Ω_2 ($\times 10^{-20}\,cm^2$)	Ω_4 ($\times 10^{-20}\,cm^2$)	Ω_6 ($\times 10^{-20}\,cm^2$)
TeO_2	WO_3	Tm_2O_3			
85	15	1	6.8	2.0	2.2
75	25	1	8.6	2.7	2.3
70	30	1	9.7	2.6	2.3

Table 3

Measured and calculated oscillator strengths of Tm^{3+} in (a) $0.15WO_3 + 0.85TeO_2$, (b) $0.25WO_3 + 0.75TeO_2$ and (c) $0.3WO_3 + 0.75TeO_2$ glass (all transitions are from the $^3H_6$ ground level to the level indicated)

Level	Wavelength (nm)	Average frequency ($\times 10^{-3}$ cm^{-1})	$\int \mu(\lambda)\,d\lambda$ ($\times 10^{-6}$)			Residual ($\times 10^{-6}$)
			Measured	Calculated		
			f_{ed}	f_{md} [36]	f_{ed}	
(a) $0.15WO_3 + 0.85TeO_2$						
$^3F_2$	660	15.150	7.3[a]	0	7.9[a]	−0.6
$^3F_3$	687	14.560	7.3[a]	0	7.9[a]	−0.6
$^3F_4$	793	12.610	8.9	0	9.2	−0.30
$^3H_5$	1212	8.250	12.6	0.9	11.8	0.8
$^3H_4$	1701	5.880	35.7	0	35.7	0.0
(b) $0.25WO_3 + 0.75TeO_2$						
$^3F_2$	661	15.130	7.7[b]	0	8.1[b]	−0.4
$^3F_3$	688	14.530	7.7[b]	0	8.1[b]	−0.4
$^3F_4$	793	12.610	10.0	0	10.3	−0.3
$^3H_5$	1211	8.260	14.0	0.9	13.4	0.6
$^3H_4$	1699	5.890	43.6	0	43.6	0.0
(c) $0.3WO_3 + 0.75TeO_2$						
$^3F_2$	661	15.130	7.5[c]	0	8.4[c]	−0.9
$^3F_3$	687	14.560	7.5[c]	0	8.4[c]	−0.9
$^3F_4$	793	12.610	10.3	0	10.7	−0.4
$^3H_5$	1211	8.260	14.9	0.86	13.8	1.1
$^3H_4$	1697	5.890	47.2	0	47.3	−0.1

[a] The oscillator strengths given for $^3F_2$ and $^3F_3$ levels are the sum of the two strengths; RMS = 1.2×10^{-6}.

[b] The oscillator strengths given for $^3F_2$ and $^3F_3$ levels are the sum of the two strengths; RMS = 0.9×10^{-6}.

[c] The oscillator strengths given for $^3F_2$ and $^3F_3$ levels are the sum of the two strengths; RMS = 1.7183×10^{-6}.

where $\bar{v}$ is the mean wave-number of the transition. Total spontaneous emission probability, W_R, for an ith excited state is given as the sum of the $A(J, J')$ terms calculated over all terminal states which is related to the radiative lifetime τ_R and the branching ratios, β, of the level by

$$\frac{1}{\tau_R(i)} = \sum_j A(i, j) = W_R,$$

and

$$\beta = \frac{A(J, J')}{W_R}. \quad (6)$$

Spontaneous luminescence probabilities (A_{ed}), radiative transition rates (τ_r), and branching ratios (β) for the metastable levels of Tm^{3+} in the $(1-x)TeO_2 + (x)WO_3$ glasses with $x = 0.15, 0.25$ and 0.30 mol were determined using Eq. (6) and are listed in Tables 4a–c.

The $^3H_6 \rightarrow {}^3H_5$ transition of Tm^{3+} ion in a glass matrix is mainly due to the magnetic dipole interaction hence the sharper peak for the absorption band is observed. In order to get broader absorption spectra it is necessary to increase relative contribution of the electric dipole transition, inhomogeneous broadening and also the sensitivity to the local field [2]. While the cross-section of the transitions due to the magnetic dipole interaction is independent of the ligand field, those due to the electric dipole interaction vary with the ligand field. According to the Judd–Ofelt theory, the line strength of the 650 nm absorption and the 1.9 μm and 478 nm emissions due to the electric dipole interaction are

Table 4
Calculated spontaneous emission probabilities, A_{ed}, radiative lifetimes, τ_R, and the branching ratios, β for Tm^{3+} in (a) $0.15WO_3 + 0.85TeO_2$, (b) $0.25WO_3 + 0.75TeO_2$ and (c) $0.3WO_3 + 0.7TeO_2$ glass

Transition	Average frequency (cm^{-1})	A_{ed} (s^{-1})	τ_R (ms)	β
(a) $0.15WO_3 + 0.85TeO_2$				
$^1G_4 \rightarrow {}^3H_6$	21277	3986	0.114	0.454
$^3H_4$	15387	615		0.072
$^3H_5$	13025.8	2896		0.332
$^3F_4$	8682	1007		0.114
$^3F_3$	6741.7	210		0.024
$^3F_2$	6216.4	34		0.004
$^3F_2 \rightarrow {}^3H_6$	15151.51	2778	0.155	0.432
$^3H_4$	9272.6	2659		0.414
$^3H_5$	6900.6	911		0.142
$^3F_4$	2541.1	68		0.01
$^3F_3 \rightarrow {}^3H_6$	14556	8007	0.103	0.829
$^3H_4$	8677.1	255		0.026
$^3H_5$	6305.2	1396		0.144
$^3F_4 \rightarrow {}^3H_6$	12610.3	4903	0.185	0.909
$^3H_4$	6731.4	410		0.076
$^3H_5$	4359.5	81		0.014
$^3H_4 \rightarrow {}^3H_6$	5878.9	1035	0.966	1.000
(b) $0.25WO_3 + 0.75TeO_2$				
$^1G_4 \rightarrow {}^3H_6$	21277	5029	0.095	0.479
$^3H_4$	15387	697		0.066
$^3H_5$	13025.8	3264		0.312
$^3F_4$	8682	1190		0.114
$^3F_3$	6741.7	234		0.023
$^3F_2$	6216.4	66		0.006
$^3F_2 \rightarrow {}^3H_6$	15128.6	2980	0.133	0.398
$^3H_4$	9242.8	3380		0.451
$^3H_5$	6870.9	1039		0.14
$^3F_4$	2518.3	85		0.011
$^3F_3 \rightarrow {}^3H_6$	14535.9	90102	0.09	0.815
$^3H_4$	8649.1	276		0.024
$^3H_5$	6277.2	1781		0.159
$^3F_4 \rightarrow {}^3H_6$	12610.3	5914	0.153	0.906
$^3H_4$	6724.5	503		0.077
$^3H_5$	4352.7	103		0.015
$^3H_4 \rightarrow {}^3H_6$	5885.8	1325	0.754	1.000
(c) $0.3WO_3 + 0.75TeO_2$				
$^1G_4 \rightarrow {}^3H_6$	21277	5397	0.092	0.496
$^3H_4$	15387	675		0.062
$^3H_5$	13025.8	3257		0.300
$^3F_4$	8682	1253		0.115
$^3F_3$	6741.7	224		0.022
$^3F_2$	6216.4	64.7		0.005
$^3F_2 \rightarrow {}^3H_6$	15128.6	2704	0.134	0.367
$^3H_4$	9235.8	3666		0.493
$^3H_5$	6871	942		0.129
$^3F_4$	2518.6	91		0.012
$^3F_3 \rightarrow {}^3H_6$	14556	8440	0.094	0.793
$^3H_4$	8663.3	255		0.023
$^3H_5$	6298.4	1944		0.182

Table 4 (*continued*)

Transition	Average frequency (cm^{-1})	A_{ed} (s^{-1})	τ_R (ms)	β
$^3F_4 \to {}^3H_6$	12610.3	6036	0.15	0.907
$^3H_4$	6717.6	515		0.077
$^3H_5$	4352.7	100		0.015
$^3H_4 \to {}^3H_6$	5892.7	1393	0.717	1.000

given by

$$S^{ed}[^3H_6 \to {}^3F_{2,3}] = 0.0\Omega_2 + 0.3164\Omega_4 + 1.1992\Omega_6,$$

$$S^{ed}[^3H_4 \to {}^3H_6] = 0.5589\Omega_2 + 0.7462\Omega_4 + 0.2574\Omega_6,$$

$$S^{ed}[^1G_4 \to {}^3H_6] = 0.0452\Omega_2 + 0.0694\Omega_4 + 0.0122\Omega_6,$$

where the three coefficients of Ω_t's are the reduced matrix elements of the unit tensor operators, $U^{(t)}$, and coefficients Ω_t ($t = 2, 4, 6$), are the intensity parameters. Strongest dependence was observed for the parameter Ω_2. On the other hand the parameters Ω_4 and Ω_6 both slowly increase first and, then decrease with increasing WO_3 content. The value of the parameter Ω_2 is determined to be 1.40 times higher when the WO_3 content in the matrix was varied from 0.15 to 0.30 mol, hence the strongest dependence on the modifier content in this matrix was observed for the parameter Ω_2. According to Judd–Ofelt theory, the intensity parameters contain two terms; one is the crystal field parameters determining the symmetry and distortion which is related to the structural change in the vicinity of Tm^{3+} ions. The second term is the covalency between the rare-earth ion and the oxygen ion for oxide glasses which is related to the radial integral of the wave functions between 4f and admixing levels, e.g. 5d, 5g and the energy denominator between these two levels. The magnetic dipole contribution to the line strength of the $^3H_6 \to {}^3H_5$ transition is constant and independent of the ligand fields as expected. However, the electric dipole contribution in the $TeO_2 + WO_3$ glass is varied with the host composition and structure, where Ω_2 and Ω_4 parameters are dominant for the $^3H_4 \to {}^3H_6$ and $^1G_4 \to {}^3H_6$ transitions that are the possible laser transitions of Tm^{3+} ion in the infrared and blue light region, respectively.

3.2. Stimulated emission cross-sections and temperature effect

Luminescence spectra of all the thulium doped glasses discussed previously were measured upon 457.9 nm laser light at 300 and 9 K. The effect of the composition on the luminescence band structure and the intensities at room temperature are presented in Fig. 3. The electronic transitions giving rise to each of luminescence bands are also shown. The full-width at half-maximum luminescence intensity of each broad band and the peak positions remain practically unchanged while the integrated luminescence intensity of each band varies with the glass composition as seen in Fig. 4. Integrated intensity of the emissions due to the $^1G_4 \to {}^3H_6$ and $^1G_4 \to {}^3H_4$ transitions first show a decrease and then an increase with increasing amount of WO_3 content. However the integrated intensity of the emission due to the $^1G_4 \to {}^3H_5$ transition shows a different dependence such that it decreases with increasing amount of WO_3 content. According to the Judd–Ofelt theory, the line strength of the first two spontaneous emissions are given by

$$S^{ed}[^1G_4 \to {}^3H_6] = 0.0452\Omega_2 + 0.0694\Omega_4 + 0.0122\Omega_6,$$

$$S^{ed}[^1G_4 \to {}^3H_4] = 0.0042\Omega_2 + 0.0186\Omega_4 + 0.0642\Omega_6.$$

Both transitions are dependent on the Ω_2 and Ω_4 since Ω_6 is found to be independent of the host composition in our glasses. The relationship between the integrated luminescence intensity ratio of $I(476 \text{ nm})/I(651 \text{ nm})$ and the ratio of the intensity parameters Ω_2/Ω_4 are given in Fig. 5. It can be seen from the figure that both ratios have a good correlation supporting the validity of the Judd–Ofelt analyses in the present study.
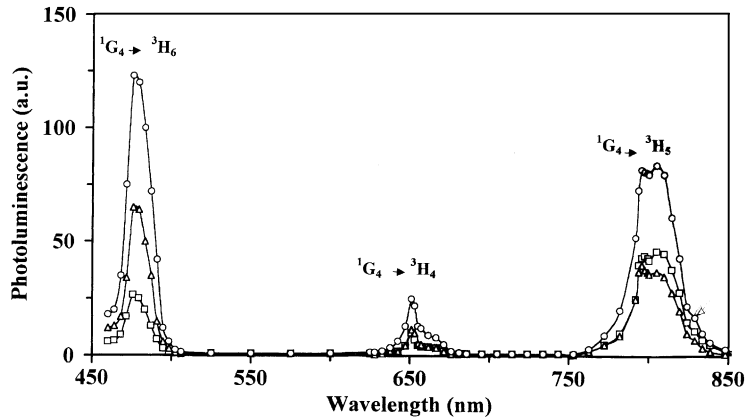
Fig. 3. Effect of composition on the spectral profiles of the luminescence bands at room temperature (excitation was into the $^1G_4$ level of Tm^{3+} ion with a laser tuned at 457.9 nm). □: 0.15 mol; △: 0.25 mol; and ○: 0.30 mol WO_3 content).
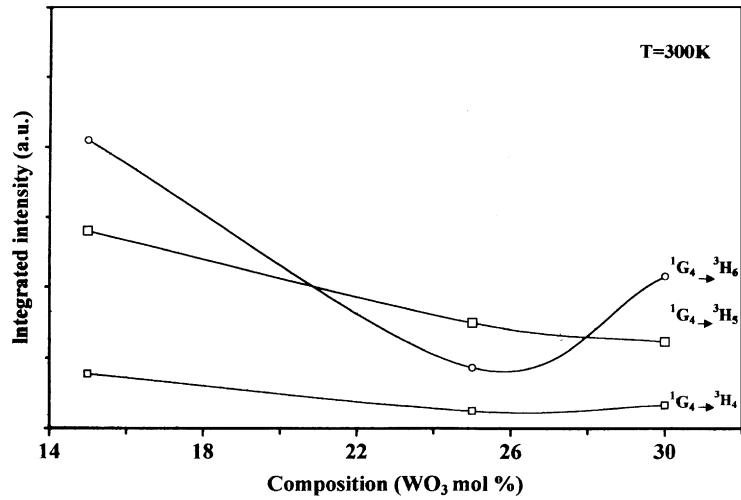

Fig. 4. Effect of composition on the integrated intensity of the luminescence bands at room temperature (excitation was into the $^1G_4$ level of Tm^{3+} ion with a laser tuned at 457.9 nm).

Stimulated emission cross-section at the peak wavelength of the emission bands observed upon 457.9 nm laser light excitation, $\sigma(\lambda_p)$, was determined from its relationship with the spontaneous emission probabilities and bandwidth, given by the formula [40];

$$\sigma(\lambda_p) = \frac{\lambda_p^4}{8\pi cn^2 \Delta\lambda_{eff}} A^{ed},$$

where n is the refractive index of the glass at λ_p and $\Delta\lambda_{eff}$ is the effective bandwidth of the respective emission band. Dependence of the stimulated emission cross-sections on the composition is presented in Table 5.

The effect of temperature on the spectral profiles of the emissions due to the $^1G_4 \rightarrow ^3H_6$ and $^1G_4 \rightarrow ^3H_5$ transitions is presented in Fig. 6. Half bandwidth of the emission due to the latter
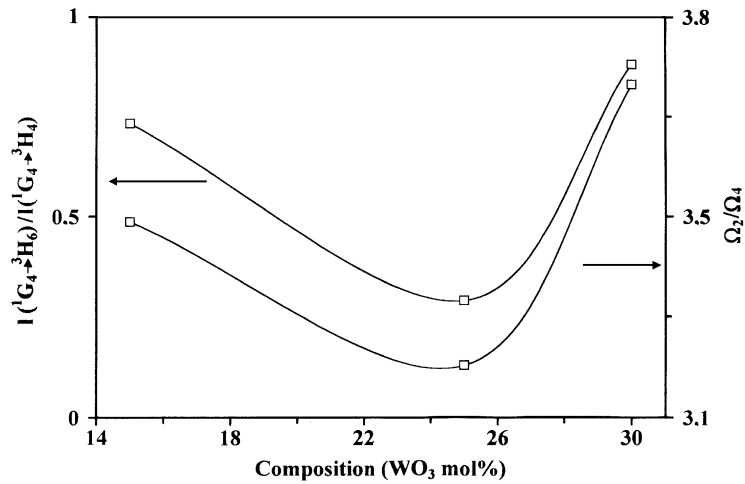
Fig. 5. Effect of composition on the integrated luminescence intensity ratio of the $I(^1G_4 \rightarrow ^3H_6)/I(^1G_4 \rightarrow ^3H_4)$ at room temperature and the ratio of Judd–Ofelt intensity parameters Ω_2/Ω_4.

Table 5
Stimulated emission cross-sections of the emissions, σ_{se}, of Tm^{3+} in $(x)WO_3 + (1-x)TeO_2$ glass observed upon 478.9 nm laser light excitation

Glass composition (mol%)			σ_{se} ($\times 10^{-21}$ cm^2)		
TeO$_2$	WO$_3$	Tm$_2$O$_3$	$^1G_4 \rightarrow ^3H_6$	$^1G_4 \rightarrow ^3H_4$	$^1G_4 \rightarrow ^3H_5$
$T = 300$ K					
85	15	1	3.9	5.8	7.5
75	25	1	4.3	2.4	1.3
70	30	1	4.5	2.1	1.2
$T = 10$ K					
85	15	1	4.2	7.5	23.1
75	25	1	7.3	3.8	22.8
70	30	1	7.9	8.2	22.7

transition becomes broad at room temperature while its peak position does not change. However, the half bandwidth of the emission band due to the $^1G_4 \rightarrow ^3H_6$ transition originating from the same level as the emission due to the $^1G_4 \rightarrow ^3H_5$ transition is found to be temperature independent while its peak wavelength shifts to shorter wavelength at room temperature. This shift may be due to the temperature effect on the terminal level for this transition which is the ground level of Tm^{3+} ion.

3.3. Local environment of Tm^{3+} ion

The decay rate of an excited state population, $W_M = 1/\tau_M$ is comprised of two processes: the intrinsic radiative decay rate ($W_R = 1/\tau_R$) and the nonradiative decay rate (W_{NR}) due to multiphonon loss. The radiative decay rate is influenced by the variations of the local crystal field symmetry at the rare-earth site. These variations are determined by the host matrix into which the ion is placed. In addition to changes in
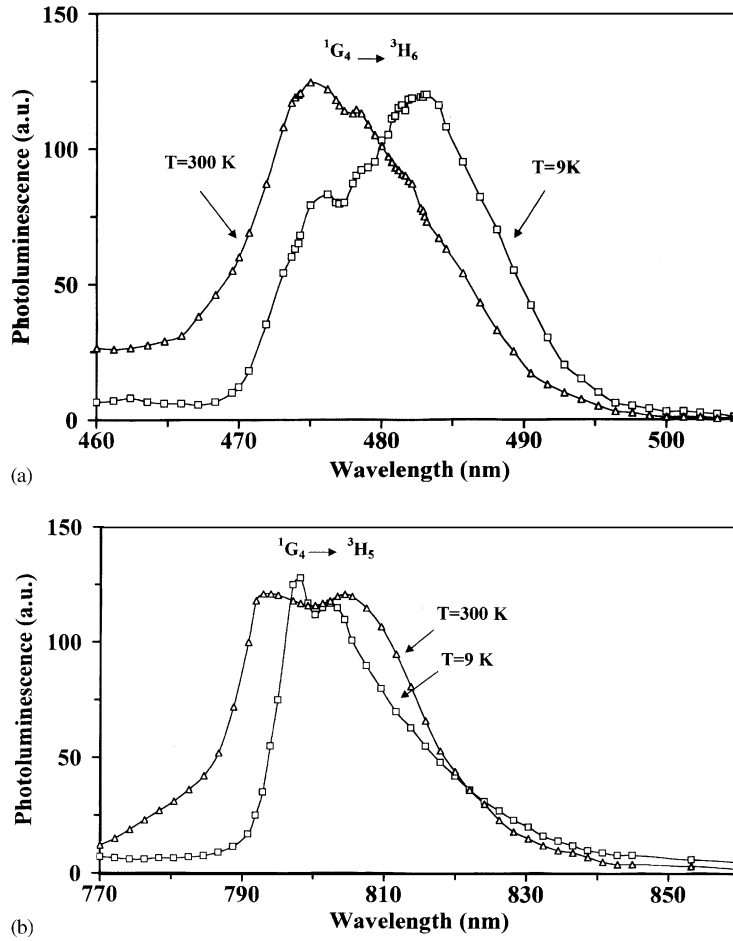
Fig. 6. Effect of temperature on the spectral profiles of the luminescence bands due to (a) $^1G_4 \rightarrow {}^3H_6$ and (b) $^1G_4 \rightarrow {}^3H_5$ transitions in $0.75TeO_2 + 0.25WO_3$ glass.

field symmetry, the local vibrational density of states of the host also provides a mechanism for depopulation of the excited state energy [38]. Electron–phonon coupling allows an excited rare-earth ion to decay nonradiatively via the production of lattice vibrations. This nonradiative process from the upper level is unattractive for amplifying devices which rely on achieving and maintaining a population inversion.

The total decay rate is thus

$$W_M = W_R + W_{NR} + W_E, \qquad (9)$$

where W_E represents an additional nonradiative loss mechanism due to the energy transfer between

the rare-earth ions. For low rare-earth ion concentrations, as it is in this study, this third process can be neglected.

Determination of the radiative decay rate, W_R, for each transition of Tm^{3+} in $TeO_2 + WO_3$ glass was accomplished using a Judd–Ofelt analysis of the absorption spectra as discussed in detail in Section 3.1.

Raman scattering spectra of the undoped glasses together with that of the α-TeO_2 crystal [39] are presented in Fig. 7. The intense broad band at $660 \, cm^{-1}$ with a shoulder at around $770 \, cm^{-1}$ dominates the Raman spectrum of each glass. Three bands with smaller intensity at 470, 355 and
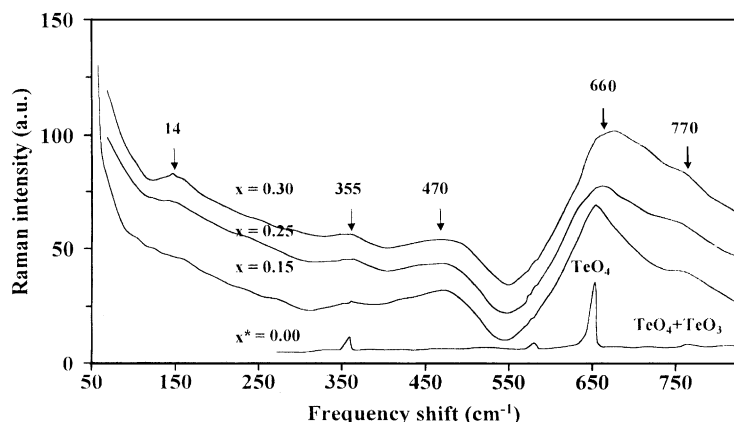
Fig. 7. Effect of composition on the Raman spectrum of TeO_2 + WO_3 glasses (*: Ref. [35]).

$140 \, cm^{-1}$ are also observed in all the glasses. The relative peak intensity of all the bands except that at $140 \, cm^{-1}$ decreases with increasing amount of WO_3. This means that addition of WO_3 into TeO_2 results in the reduction of Te–O–Te linkages, and the formation of W–O–W and W–O–Te linkages as was also observed by other researchers [40].

The presence of high-energy stretching vibrations of the network in many oxide glasses lowers the efficiency of both Stokes and anti-Stokes (upconversion) luminescence. However, the phonon cut-off frequency of our glasses, which is about $770 \, cm^{-1}$ according to the Raman spectra given in Fig. 7, is lower than that of fluorophosphate glasses which is $1060 \, cm^{-1}$ [40]. Therefore, it can be concluded that the tellurite glasses modified with WO_3 are better candidates for upconversion luminescence originating from the $^1G_4$ level of Tm^{3+} ion.

4. Conclusions

Effect of WO_3 content on the spontaneous emission probabilities, stimulated emission cross-sections and the local environment of Tm^{3+} ion in $(1-x)TeO_2 + (x)WO_3$ binary glasses have been investigated. The results obtained are summarised as follows:

(1) Value for the integrated absorption cross-section for each ground state transitions of Tm^{3+}, except that of $^3H_5$ level, in the visible and near infrared wavelength region changes with the WO_3 content.

(2) Value of the Ω_2-Judd–Ofelt intensity parameter determined using electric dipole–dipole type transitions shows the strongest dependence on the host composition and it increases with the increasing WO_3 amount. The value of the Ω_4 increases rather slowly while the value of Ω_6 is practically independent of the composition. The strong dependence of the parameter Ω_2 indicates that this parameter is related to the structural change and the symmetry of the local environment of the Tm^{3+} ions in this matrix.

(3) According to the Judd–Ofelt theory, the $^1G_4 \rightarrow {}^3H_6$ transition has the highest branching ratio with the value of about 50% in all the glasses. This result agrees with the results obtained by comparing the relative integrated luminescence intensities of the transitions observed in the 450 and 900 nm wavelength region upon 457.9 nm laser light excitation (Fig. 3).

(4) The radiative lifetime τ_R, of the infrared luminescence is may be due to the $^3H_4 \rightarrow {}^3H_6$ transition decreases from 966 to 717 μs when WO_3 content is increased from 0.15 to 0.30 mol. The best composition for this luminescence is therefore, that of containing the least amount of WO_3 when it is considered as a possible laser transition in the TeO_2–WO_3 binary glass system.

(5) The behaviour of the ratio of the luminescence intensities due to the $^1G_4 \rightarrow {}^3H_6$ and $^1G_4 \rightarrow {}^3H_4$ transitions can be explained by variation of the ratio of the Judd–Ofelt intensity parameters, Ω_2/Ω_4, with the glass composition.

(6) Blue shift for the luminescence peaking at about 475 nm at room temperature due to the $^1G_4 \rightarrow {}^3H_6$ transition was observed while no shift at the maximum luminescence wavelength of the luminescence peaking at about 800 nm due to the $^1G_4 \rightarrow {}^3H_5$ transition was observed. This indicates that the blue shift observed for the former emission is may be due to the thermal effect on the terminal level that happens to be the ground level of the Tm^{3+} ion.

(7) The energy gap between the $^1G_4$ and the next low lying level $^3F_2$ levels of Tm^{3+} ion has determined from the absorption measurements to be $\Delta E = 6125 \, cm^{-1}$. According to the Raman scattering measurements, the maximum phonon band was observed at $760 \, cm^{-1}$ for these glasses. Combining these two results it may be said that the one phonon assisted nonradiative transition from the $^1G_4$ level should be less probable.

As a result, it can be concluded from our data that Tm^{3+} doped TeO_2–WO_3 glasses are promising materials for the infrared amplifiers as well as the blue up-conversion lasers when the wavelength of the pumping light is chosen as 650 nm.

References

[1] V.D. Rodriguez, V. Lavin, U.R. Rodriguez-Mendoza, I.R. Martin, Opt. Mater. 13 (1999) 1.
[2] S. Tanabe, J. Non-Cryst. Solids 259 (1999) 1.
[3] H. Takebe, K. Yoshino, T. Murata, K. Morinaga, J. Hector, W.S. Brocklesby, D.W. Hewak, J. Wang, D.N. Payne, Appl. Opt. 36 (24) (1997) 5839.
[4] S. Tanabe, K. Hirao, N. Soga, J. Non-Cryst. Solids 122 (1990) 79.
[5] J.C. Michel, D. Morin, F. Auzel, Rev. Phys. Appl. 13 (1978) 859.
[6] D.L. Sidebottom, M.A. Hruschka, B.G.B. Potter, R.K. Brow, J. Non-Cryst. Solids 222 (1997) 282.
[7] J.E. Stanworth, J. Soc. Glass Technol. 36 (1952) 217.
[8] J.E. Stanworth, J. Soc. Glass Technol. 36 (1954) 425.
[9] J.E. Stanworth, Nature 169 (1952) 581.
[10] M.J. Weber, J.D. Myers, D.H. Bluckburn, J. Appl. Phys. 52 (4) (1981) 2944.
[11] D.R. Ulrich, J. Am. Ceram. Soc. 47 (1964) 595.
[12] J.S. Wang, E.M. Vogel, E. Snitzer, Opt. Mater. 3 (1994) 187.
[13] S.H. Kim, T. Yoko, J. Am. Ceram. Soc. 78 (4) (1995) 1061.
[14] H. Burger, W. Vogel, V. Kozhukharov, Infrared Phys. 25 (1985) 395.
[15] G. Özen, J.-P. Denis, M. Genotelle, F. Pellé, J. Phys.: Condens. Matter. 7 (1995) 4325.
[16] H. Takebe, Y. Nageno, K. Morinaga, J. Am. Ceram. Soc. 77 (8) (1994) 2132.
[17] B.R. Judd, Phys. Rev. 127 (1962) 750.
[18] G.S. Ofelt, J. Chem. Phys. 37 (1962) 511.
[19] H. Takebe, Y. Nageno, K. Morinaga, J. Am. Ceram. Soc. 78 (5) (1995) 1161.
[20] B. Cleska, D. Ronarc̀h, D. Bayart, Y. Sorel, L. Hamon, M. Guibert, J.L. Beylat, J.F. Kerdiles, M. Semenkoff, IEEE Trans. Photon. Technol. Lett. 6 (1994) 509.
[21] K. Oh, A. Kilian, T.F. Morse, J. Non-Cryst. Solids 259 (1999) 10.
[22] P. Wysocki, T. Rench, M. Andrejco, D. DiGiovanni, I. Jayawardene, Optical Fiber Communication Conference (OFC) Vol. 6, OSA Technical Digest Series, Paper WF2, 1997.
[23] A. Mori, Y. Ohishi, Optical Fiber Communication Conference (OFC) Vol. 6, OSA Technical Digest Series, Paper WA1, 1998.
[24] T. Kosuge, Y. Bening, V. Dimitriov, R. Sato, T. Komatsu, J. Non-Cryst. Solids 242 (1998) 154.
[25] K. Tanaka, T. Yoko, H. Yamada, K. Kamiya, J. Non-Cryst. Solids 103 (1988) 250.
[26] R.N. Sinclair, A.C. Wright, B. Bachra, Y.B. Dimitriev, V.V. Dimitriov, M.G. Arnaudov, J. Non-Cryst. Solids 232-234 (1998) 38.
[27] J.M. Reau, B. Tanguy, J. Portier, J.M. Rojo, J. Sana, M.P. Herrero, J. Phys. IV 2 (1992) 165.
[28] S. Neov, I. Gerasimova, V. Kozhukharov, M. Marinov, J. Mater. Sci. 15 (1980) 1153.
[29] A.K. Yakhkind, J. Am. Ceram. Soc. 49 (12) (1966) 670.
[30] V.R. Kumar, N. Veeraiah, B.A. Rao, S. Bhuddudu, J. Mater. Sci. 33 (1998) 2659.
[31] A.A. Bahgdat, E.E. Shaisha, A.I. Sabry, J. Mater. Sci. 22 (1987) 1323.
[32] T. Murata, H. Takebe, K. Morinaga, J. Am. Ceram. Soc. 80 (1) (1998) 249.
[33] M.L. Öveçoğlu, G. Özen, B. Demirata, A. Genc, J. Euro. Ceram. Soc. 21 (2001) 177.
[34] P.A.V. Johnson, A.C. Wright, C.A. Yarker, R.N. Sincair, J. Non-Cryst. Solids 81 (1986) 163.
[35] E.W.J. Oomen, J. Lumin. 50 (1992) 317.
[36] J.R. Lincoln, W.S. Brocklesby, F. Cusso, J.E. Townsend, A.C. Tropper, A. Pearson, J. Lumin. 50 (1991) 297.

[37] A.A. Kaminskii, Crystalline Lasers: Physical Processes and Operating Schemes, CRC Press, Boca Raton, FL, 1996.

[38] W.F. Krupke, IEEE J. Quant. Electron QR-10 (1974) 450.

[39] F.C. Cassanjes, Y. Messaddeq, L.F.C. deOliveira, L.C. Courrol, L. Gomes, S.J.L. Ribeiro, J. Non-Cryst. Solids 247 (1999) 58.

[40] T. Sekiya, N. Mochida, S. Ogawa, J. Non-Cryst. Solids 176 (1994) 105.